Collision-Induced Dissociation and Theoretical Studies of Cu^+−Dimethyl Ether Complexes†

Hideya Koizumi, Xiao-Guang Zhang, and P. B. Armentrout*

Department of Chemistry, University of Utah, Salt Lake City, Utah 84112

Received: September 27, 2000; In Final Form: December 20, 2000

Collision-induced dissociation of the $Cu^+(DME)_n$ complexes for $n = 1-4$ is studied using kinetic energy dependent guided ion beam mass spectrometry. In all cases, the primary products involve the loss of one dimethyl ether (DME) from the complex. Analysis of the kinetic energy dependent cross sections yields absolute bond dissociation energies for these complexes of 1.92 ± 0.12, 2.00 ± 0.08, 0.57 ± 0.04, and 0.47 ± 0.10 eV for $n = 1-4$, respectively. These values are compared with theoretical values obtained using density functional theory and ab initio calculations at second and fourth order Møller−Plesset perturbation, MP2, and MP4(SDTQ) levels. Our results are compared with previously studied alkali cation-ether complexes and with metal−water ligand systems. Although Cu^+ and all alkali cations have ^1S electronic ground states, the comparison shows different trends for Cu^+ because of hybridization effects involving the valence d-electrons.

I. Introduction

Noncovalent interactions play a significant role in molecular recognition. Such interactions involve a subtle interplay of entropic and enthalpic effects that are difficult to separate. Gas-phase data on such systems are one means of elucidating these effects and providing fundamental insight into the basis of molecular recognition. Our studies are motivated by an interest in developing the principals of molecular recognition for use in advanced chemical separations[1] and analytical methodology.[2] Previously, we have examined noncovalent interactions between alkali ions and neutral molecules such as dimethyl ether and water, both simple monodentate ligands,[3−8] as well as with crown ethers.[4−7,9] The alkali metal ions have spherically symmetric ^1S electronic ground states, as do singly charged ions of the coinage metals. However, the metal ligand interactions, which can be described as mostly electrostatic, are stronger for coinage ion water clusters compared to alkali metal water clusters, as several groups have reported.[10−13] Bauschlicher and co-workers investigated Cu^+ water clusters using restricted Hartree−Fock (RHF) and modified coupled-pair functional (MCPF) theories.[10] Recently, Feller and co-workers studied coinage metal cation water clusters using complete basis set coupled cluster techniques.[11] The results of these calculations are in good agreement with previous experimental results for $Cu^+(H_2O)_n$, $n = 1-4$, complexes.[12,13]

In this project, we investigate the binding of Cu^+ to 1−4 dimethyl ether (DME) molecules. Guided ion beam mass spectrometry is used to measure the kinetic energy dependent cross sections for collision-induced dissociation (CID). Analysis of these results provides absolute binding energies of these complexes after consideration of reactant energy distributions, effects of multiple collisions, and lifetime effects. These results are compared to cost-effective theoretical results, which become considerably more expensive as the size of the Cu^+ ion dimethyl ether complexes become larger. The binding energies of these complexes are compared to analogous alkali metal complexes to show how the valence d electrons change the metal−ligand interactions. Trends in the thermochemistry for dimethyl ether and H_2O clusters are also compared.

II. Experimental and Theoretical Methods

A. Experimental Approach. For all reactions studied here, cross sections are collected using a guided ion beam tandem mass spectrometer described previously.[14,15] $Cu^+(DME)_n$ complexes are produced in a dc discharge flow tube ion source. At the front end of a meter long flow tube, a dc discharge in a ~10% mixture of Ar in He creates Ar^+ ions that sputter metal ions from a copper cathode. The overall pressure is about 0.5 Torr and typical operating conditions of the dc discharge are 1.3 kV and 30 mA. DME molecules are introduced about 50 cm downstream of the source and attached to the copper ions by three-body condensation. While the complexes traverse the remainder of the flow tube, they are thermalized by undergoing $> 10^4$ collisions with the bath gases. The assumption of efficient thermalization is reasonable, as suggested by previous work.[12,16−18]

These ions are extracted from the source, accelerated, and focused into a magnetic sector momentum analyzer for mass analysis. The mass-selected ions are slowed to a desired kinetic energy and focused into an rf octopole ion guide.[19] The guide passes through a static gas cell containing xenon gas, used in our CID studies for reasons described elsewhere.[12,20] After exiting the gas cell, the product and remaining reactant ions drift to the end of the octopole, where they are extracted and focused into a quadrupole mass filter for mass analysis. A secondary electron scintillation ion counter detects the mass-analyzed reactant and product ions. These signals are converted to absolute reaction cross sections as described previously.[12] Absolute uncertainties in these cross sections are estimated to be ±20%.

Sharp features in observed cross sections are broadened by thermal motion of the xenon gas and the distribution of ion energies. The distribution and absolute zero of the ion kinetic energies are measured using the octopole as a retarding potential analyzer.[12] The uncertainty in the absolute energy scale is ±0.05 eV (lab). Typical distributions have a full width at half-maximum (fwhm) between 0.4 and 0.8 eV (lab). Kinetic

† Part of the special issue "Aron Kuppermann Festschrift".

10.1021/jp003509p CCC: $20.00
Published on Web 02/14/2001

TABLE 1: Vibrational Frequencies and Internal Energies of $Cu^+((dme)_n$ Complexes[a]

species[b]	E_{vib} (eV)[c]	frequencies (cm^{-1})
DME [C_{2v}]	0.04	188, 234, 392, 926, 1096, 1139, 1170, 1201, 1246, 1434, 1459, 1465, 1468, 1469, 1482, 2827, 2840, 2872(2), 2952, 2954
Cu^+(DME) [C_{2v}]	0.10 (0.01)	73, 137, 138, 213, 235, 422, 868, 1033, 1130, 1155, 1163, 1252, 1435, 1448, 1461, 1463, 1470, 1474, 2892, 2897, 2974, 2975, 2981, 2983
$Cu^+(DME)_2$ [D_{2d}]	0.25 (0.03)	13, 37(2), 71(2), 140, 141, 151(2), 158, 236(2), 258, 418, 433, 876, 881, 1044(2), 1132(2), 1159(2), 1165(2), 1254, 1255, 1435(2), 1450, 1451, 1463(2), 1464(2), 1471(2), 1475(2), 2889(2), 2893, 2894, 2965(2), 2966(2), 2981(2), 2983(2)
$Cu^+(DME)_3$ [D_3]	0.46 (0.04)	14(2), 21(2), 30(2), 63(2), 70, 122(2), 129, 139, 155(3), 173(2), 234(3), 411(2), 413, 886(2), 900, 1062, 1063(2), 1134(3), 1165, 1166(5), 1253(3), 1435, 1436(2), 1453(2), 1455, 1464, 1465(2), 1466, 1467(2), 1470(4), 1477(3), 1478, 2876, 2877(2), 2883(2), 2884, 2946(6), 2972(3), 2973(3)
$Cu^+(DME)_4$ [S_4]	0.64 (0.05)	14(2), 17, 21, 30, 34, 39(2), 40, 62, 63, 65(2), 107, 109(2), 118, 126, 139, 140(2), 163, 165(2), 166, 233(3), 235, 406(3), 409, 894(3), 911, 1071(3), 1072, 1136(4), 1167(4), 1170, 1171(2), 1172, 1252(4), 1434(3), 1436, 1455(3), 1458, 1466(3), 1468(5), 1469, 1470(2), 1471, 1479(3), 1480, 2868(3), 2869, 2876(3), 2878, 2931(6), 2932, 2969(2), 2970(2), 2972(4)

[a] Vibrational frequencies are calculated at the RHF/6-31+G* level and scaled by 0.8929. Degeneracies in parentheses. [b] Symmetries of each species are listed in brackets. [c] Average vibrational energies at 298 K.

energies in the laboratory frame are converted to ion energies in the center-of-mass (CM) flame by $E(CM) = E(lab)\, m/(M + m)$, where M and m are ion and neutral reactant masses, respectively. All energies cited in this paper are in the CM frame except as noted.

B. Theoretical Methods. The geometries, vibrational frequencies, and binding energies of the $Cu^+(DME)_n$ complexes for $n = 1-4$ are calculated using Gaussian 98 programs.[21] Geometries are initially optimized by ab initio restricted Hartree−Fock (RHF) methods using the 6-31+G* basis set. At this level, the symmetries of the ground states for $n = 1-4$ are found to be C_{2v}, D_{2d}, D_3, and S_4, respectively. Similar geometries were reported for $Cu^+(H_2O)_x$ complexes determined at the RHF level as reported by Bauschlicher et al..[10] for all $n = x$. For $n = 1$ and 2, we further optimized these geometries using the Becke three-parameter fit with the functional of Lee, Yang, and Parr (B3LYP),[22] the Becke three-parameter functional with nonlocal correlation provided by the Perdew 86 expression (B3P86),[23] and second-order Møller−Plesset perturbation theory, MP2.[24] In these calculations, the symmetries are fixed at those found using RHF calculations, and we use either a small hybrid (S-hybrid) basis set [6-311+G(3df) for Cu, 6-31+G* for O, C, and H] or a large hybrid (L-hybrid) basis set [6-311+G(3df) for Cu, 6-311+G* for O, 6-31+G* for C and H]. For $n = 1$, we verified that use of a 6-311++G** basis for C and H at the B3LYP and B3P86 levels did not significantly change either the geometries or BDEs. Larger basis sets on Cu and O are used because these atoms comprise the binding site in these complexes. The use of additional functions on the copper and oxygen atoms is performed in analogy with comparable augmentations in calculations of analogous $Li^+(DME)_n$ complexes.[3] In addition, Feller et al. have shown for the analogous $Cu^+(H_2O)$ complex that the use of f functions on copper are needed to adequately describe the binding.[11] We also performed additional single point calculations: MP2/S-hybrid using the B3LYP/6-31+G* and B3LYP/S-hybrid geometries, and MP4(SDTQ)/L-hybrid using optimized geometries determined at the MP2/L-hybrid level of theory.

For $n = 3$ and 4, the complex geometries are optimized at the RHF, B3LYP, and B3P86 levels of theory with either a 6-31+G* or the S-hybrid basis set to avoid calculations that are too expensive. The symmetries are fixed at those found for RHF calculations to reduce the number of steps in the optimizations. MP2 optimizations are too expensive for $n = 3$ and 4. For $n = 3$ and 4, MP2/S-hybrid single point calculations were performed using the D_3 and S_4 symmetry-restricted optimized geometries determined at the B3LYP/6-31+G* and B3LYP/S-hybrid levels.

For all complexes, harmonic frequencies of the normal modes and zero point energies (ZPEs) for all molecular species were calculated at the RHF/6-31+G* level and scaled by 0.8929.[25] These scaled frequencies are listed in Table 1. All calculated BDEs described below include ZPE corrections. In addition, most of the BDEs are corrected using the full counterpoise method of Boys and Bernardi[26] for basis set superposition error (BSSE). We find that the BSSE corrections are approximately the same for different sized complexes and are smaller for B3LYP calculations (an average of 0.07 ± 0.01 eV) than for MP2 calculations (an average of 0.22 ± 0.04 eV).

Recent MP2 studies of $Cu^+(H_2O)_x$ complexes by Feller and co-workers[11] find different conformers that are more stable than the high-symmetry geometries reported by Bauschlicher et al. for $x = 2-4$.[10] In some cases ($x = 2-4$), there are conformers that are slightly distorted from the conformers reported by Bauschlicher et al. In other cases ($x = 3$ and 4), the complexes have one or two water ligands that do not interact directly with the Cu^+ cation, again in contrast to the results of Bauschlicher et al. To explore such alternate conformers, geometry optimizations and normal-mode analysis with no symmetry restrictions were performed for $Cu^+(DME)_n$ ($n = 1-3$) complexes using both RHF and B3LYP with a 3-21G basis set. The geometries of $Cu^+(DME)_n$ for $n = 1$ and 2 were further optimized at MP2/6-31+G* and B3LYP/6-31+G* levels of theory. For $n = 3$, single point calculations using the RHF/3-21G and B3LYP/3-21G optimized geometries were performed at the MP2/3-21G level to determine the ground state conformer. Because some of these structures involve hydrogen bonding, the conclusions drawn from the use of the 3-21G basis set may not be adequate, and deserve further investigation using larger basis sets. However, such calculations are beyond our present computational facilities. The ground-state C_1 conformer and symmetric D_3 geometry of $Cu^+(DME)_3$ determined at the RHF level were further optimized at a B3LYP/6-31+G* level of theory. For both MP2/6-31+G* and B3LYP/6-31+G* optimized geometries, single point calculations at the MP2/S-hybrid level including BSSE corrections were performed. For $n = 4$, no calculations without symmetry restrictions were conducted because of the expense.

It should be noted that recent studies on the covalently bound diatomics, CuH^+ and CuO^+, suggest that MPn methods can have difficulty yielding meaningful results, a problem that may arise from instabilities in the HF wave functions.[27,28] However, no

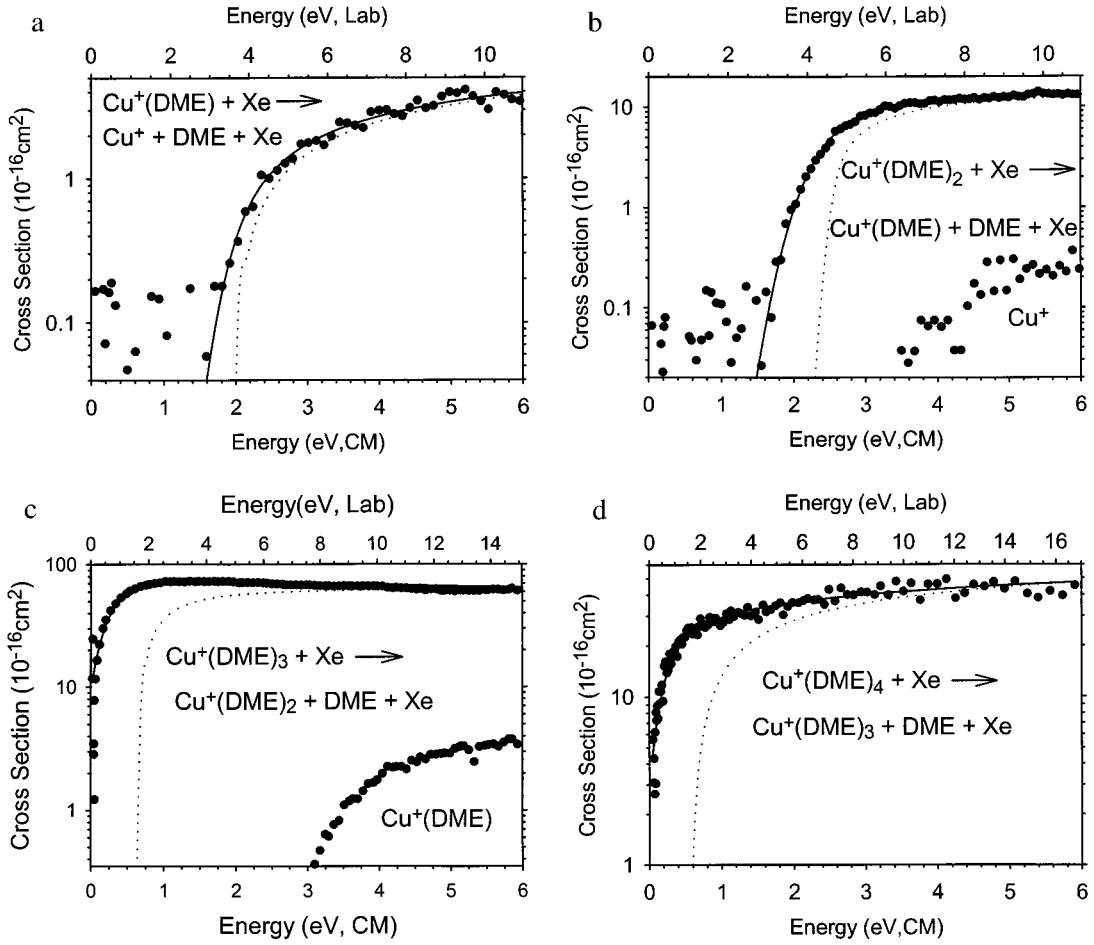

Figure 1. Cross sections for reactions of $Cu^+(DME)_n$, $n = 1-4$ (parts a−d, respectively), with xenon as a function of kinetic energy in the center-of-mass frame (lower *x* axis) and laboratory frame (upper *x*-axis). The dotted lines show the model of eq 2 for reactants with no internal energy and in the absence of kinetic energy broadening. Solid lines are this model convoluted with the internal and kinetic energy distributions of the reactants.

such problems were noted by Luna et al. for noncovalently bound Cu^+ complexes, e.g., $Cu^+(H_2O)$ and $Cu^+(NH_3)$,[28] and likewise, we did not observe such instabilities in the present study.

III. Results

A. Experimental Observations. Experimental cross sections for the collision-induced dissociation (CID) of $Cu^+(DME)_n$, $n = 1-4$, complexes with xenon are shown in Figure 1. In all cases, the primary process for all complexes is the loss of a single DME ligand in reaction 1.

$$Cu^+(DME)_n + Xe \rightarrow Cu^+(DME)_{n-1} + DME + Xe \quad (1)$$

For $n = 1$, the primary Cu^+ ion product cross section has an apparent threshold of about 1.7 eV and rises throughout the energy range examined. For $n = 2$, the primary $Cu^+(DME)$ ion product cross section has an apparent threshold near 1.7 eV and level off with a maximum magnitude of 13 Å^2. Small amounts (0.3 Å^2 maximum) of the Cu^+ secondary product are observed at higher energies starting near 3.4 eV. For $n = 3$, the $Cu^+(DME)_2$ primary product ion cross section has an apparent threshold near 0 eV. Also, small amounts of a $Cu^+(DME)$ secondary product are observed with an apparent threshold near 3 eV and a maximum magnitude of 3.5 Å^2. No Cu^+ ions are observed at any energy studied. For $n = 4$, the only product observed is $Cu^+(DME)_3$ because of the small intensity of the reactant ion beam (10^4 ion/s). Again the cross section rises rapidly once the kinetic energy is increased from thermal.

B. Thermochemical and Threshold Analysis. The kinetic energy dependence of the experimental cross sections is modeled using eq 2

$$\sigma(E) = \sigma_0 \Sigma g_i (E + E_i - E_0)^N/E \quad (2)$$

where E is the relative translational energy of the reactants, E_0 is the 0 K threshold of the reaction, σ_0 is an energy-independent scaling factor, and N is an adjustable parameter. The sum is over the ro-vibrational states of the reactant ion, having energies E_i and populations g_i (where $\Sigma g_i = 1$). The vibrational frequencies of the complexes are given in Table 1. The Beyer−Swinehart algorithm[29] is used to calculate the distribution of internal states of the complex at 300 K, the temperature of the gas in the flow tube.

To analyze the kinetic energy dependence of these cross sections and acquire accurate thermochemistry, several effects must be considered. First, the internal energy of the reactants must be well-characterized. This is achieved by the use of the flow tube ion source, yielding internal energy distributions that should be Maxwellian. Second, the collision gas must provide efficient kinetic to internal energy transfer. Using Xe gas, which is heavy and polarizable while having no internal modes to carry away energy, satisfies this condition.[12,20] Third, rigorous single collision conditions are required to avoid problems associated

TABLE 2: Parameters of eq 2 Used to Model the Data[a]

species	σ_0[b]	N[b]	E_0 (PSL) (eV)	E_0 (w/o lifetime) (eV)
Cu^+(DME)	4.2 (0.8)	1.2 (0.1)	1.92 (0.12)	1.94 (0.11)
Cu^+(DME)$_2$	29.2 (5.3)	0.8 (0.1)	2.00 (0.08)	2.48 (0.13)
Cu^+(DME)$_3$	82.9 (0.5)	0.9 (0.1)	0.57 (0.04)	0.71 (0.07)
Cu^+(DME)$_4$	36.3 (3.6)	1.2 (0.1)	0.47 (0.10)	0.78 (0.08)

[a] Uncertainties are listed in parentheses. [b] Average values for loose PSL transition state.

with depositing excess (and unknown) energy in secondary collisions. To produce rigorous single-collision conditions, data obtained at different neutral reactant pressures (∼0.05, 0.1, 0.2 mTorr) are extrapolated to zero pressure by linear regression.[30] These are the cross sections shown in Figure 1.

Fourth, because the ions move through the apparatus in a finite time (∼ 10^{-4} s), it is important to consider the lifetime of dissociating ions, particularly for large complexes such as Cu^+(DME)$_3$ or Cu^+(DME)$_4$. The lifetime effect is taken into account using Rice−Ramsperger−Kassel−Marcus (RRKM) theory[31] in the phase space limit (PSL) using equations developed by Rodgers and Armentrout.[32] Briefly, the transition state (TS) for dissociation is modeled by loosely interacting products such that both fragments are free to rotate. This PSL is appropriate for ion−molecule complexes because the TS for the reverse, barrierless association process is accurately described as lying at the top of the centrifugal barrier. In this study, the 2-D external rotations are treated adiabatically but with centrifugal effects included, consistent with the discussion of Waage and Rabinovitch.[33] The adiabatic 2-D rotational energy is treated using a statistical distribution with explicit summation over the possible values of the rotational quantum number, as described in detail elsewhere.[32]

Because the rotational, vibrational, and translational energy distributions are explicitly included in our modeling, the threshold energies determined with eq 2 correspond to 0 K. By assuming that E_0 represents the energy difference between the reactants and products at 0 K,[12] threshold energies for CID reactions are equated with 0 K bond dissociation energies (BDEs). This correspondence is generally true for ion−molecule reactions because the presence of activation barriers in excess of the reaction endothermicity is unlikely,[34,35] especially for the simple heterolytic bond cleavages considered here.[36] The reported thresholds for all reactions are determined in the following way. First, eq 2 with an initial set of parameters is convoluted with the kinetic energy distribution of the ion beam and the thermal motion of Xe gas in the reaction cell. The parameters of eq 2 are optimized using a nonlinear least-squares analysis to give a best fit to the zero pressure extrapolated cross sections. This represents the threshold energy at 0 K without lifetime corrections. The threshold energies including the PSL analysis provide the bond energy at 0 K including lifetime corrections. An estimate of the error in the threshold energy is obtained by variations in the parameter N in eq 2, variations in the time available for reaction by factors of 2 and $^1/_2$, variations in the vibrational frequencies by ±20%, and the error in the absolute energy scale (±0.05 eV lab). Threshold energies along with the optimum fitting parameters, σ_0 and N, are listed in Table 2.

Kinetic shifts, obtained from the difference in thresholds with and without lifetime effects, are 0.02, 0.48, 0.14, and 0.31 eV for n = 1−4, respectively. The trends in these kinetic shifts differ from those observed for Li^+(DME)$_x$ or Na^+(DME)$_x$ complexes,[3,4] where the lifetime corrections increase systematically for larger complexes. This latter trend simply reflects the increasing density of states of the complexes with increasing size. For Cu^+(DME)$_n$ complexes, the same pattern is observed except for Cu^+(DME)$_2$ which has a relatively high kinetic shift. This is a consequence of the much larger BDE for this complex compared with n = 3 and 4, or compared to the analogous Li^+ and Na^+ complexes.

TABLE 3: Optimized Geometrical Parameters for Cu^+(DME)$_n$ Clusters[a]

	sym-metry	method/basis[a]	Cu−O (Å)	∠COC (deg)	∠OCuO (deg)
Cu^+(DME)	C_{2v}	RHF/6-31+G*	2.029	113.2	
		RHF/L-hybrid	2.031	113.3	
		B3LYP/6-31+G*[b]	1.912	113.2	
		B3LYP/S-hybrid[b]	1.918	113.0	
		B3P86/S-hybrid[b]	1.902	112.7	
		B3LYP/L-hybrid[b]	1.920	113.1	
		B3P86/L-hybrid[b]	1.903	112.9	
		B3LYP/L-hybrid#[b]	1.920	112.9	
		B3P86/ L-hybrid#[b]	1.903	112.6	
		MP2/6-31+G*[b]	1.900	111.7	
		MP2/L-hybrid[b]	1.886	112.1	
	C_s	B3LYP/6-31+G*	1.914	118.1	
		MP2/6-31+G*	1.902	111.7	
Cu^+(DME)$_2$	D_{2d}	RHF/6-31+G*	2.009	113.3	180.0
		RHF/L-hybrid	2.013	113.5	180.0
		B3LYP/6-31+G*[b]	1.892	113.1	180.0
		B3LYP/S-hybrid[b]	1.898	113.0	180.0
		B3P86/S-hybrid[b]	1.879	112.8	180.0
		B3LYP/L-hybrid[b]	1.899	113.2	180.0
		B3P86/L-hybrid[b]	1.880	113.0	180.0
		MP2/6-31+G*[b]	1.848	112.0	180.0
		MP2/L-hybrid[b]	1.838	112.4	180.0
	C_2	B3LYP/6-31+G*	1.894	113.0	177.9
		MP2/6-31+G*	1.851	111.6	177.7
Cu^+(DME)$_3$	D_3	RHF/6-31+G*	2.143	113.4	120.0
		RHF/S-hybrid	2.148	113.4	120.0
		B3LYP/6-31+G*[b]	2.045	112.7	120.0
		B3LYP/S-hybrid[b]	2.044	112.6	120.0
		B3P86/S-hybrid[b]	2.017	112.4	120.0
	C_1	B3LYP/6-31+G*	1.964(2), 2.249	112.6	159.0, 100.5
Cu^+(DME)$_4$	S_4	RHF/6-31+G*	2.237	113.4	109.5
		RHF/S-hybrid	2.245	113.4	109.5
		B3LYP/6-31+G*[b]	2.147	112.5	109.5
		B3LYP/S-hybrid[b]	2.146	112.5	109.5
		B3P86/S-hybrid[b]	2.111	112.3	109.5

[a] S-hybrid = 6-311+G(3df) for Cu, 6-31+G* for O, C, and H. L-hybrid = 6-311+G(3df) for Cu, 6-311+G* for O, and 6-31+G* for C and H (# indicates 6-311++G** for C and H). [b] Geometry optimizations restricted to specified point group.

C. Theoretical Geometries of Cu^+(DME)$_n$ Complexes. For Cu^+(DME), the only stationary point found at the RHF/6-31+G* level was a C_{2v} structure, in which the metal ion is aligned with the dipole moment of the ligand, Figure 2a. In contrast, geometry searches at the MP2/3-21G, B3LYP/3-21G, MP2/6-31+G*, and B3LYP/6-31+G* levels of theory find the C_s structure shown in Figure 2a. The Cu^+−O bond is out of the C−O−C plane by 17.8° (21.1°) at the MP2/6-31+G* (B3LYP/6-31+G*) levels, and the MP2/6-31+G* Cu^+−O bond length (Table 3) is 0.012 Å shorter than that calculated at the B3LYP/6-31+G* level of theory. Despite these differences in the distorted geometries, the stabilization of the complex is only 0.0035 (0.0026) eV with respect to the C_{2v} geometries at the MP2/6-31+G* (B3LYP/6-31+G*) levels. Consequently, the binding energies calculated for the C_s and C_{2v} structures show negligible differences at both levels of theory. Previous G2 studies of Cu^+ complexes[28] also found nonnegligible differences in the MP2 and B3LYP optimized geometries, but found that the resultant BDEs were not sensitive to the different geometries.

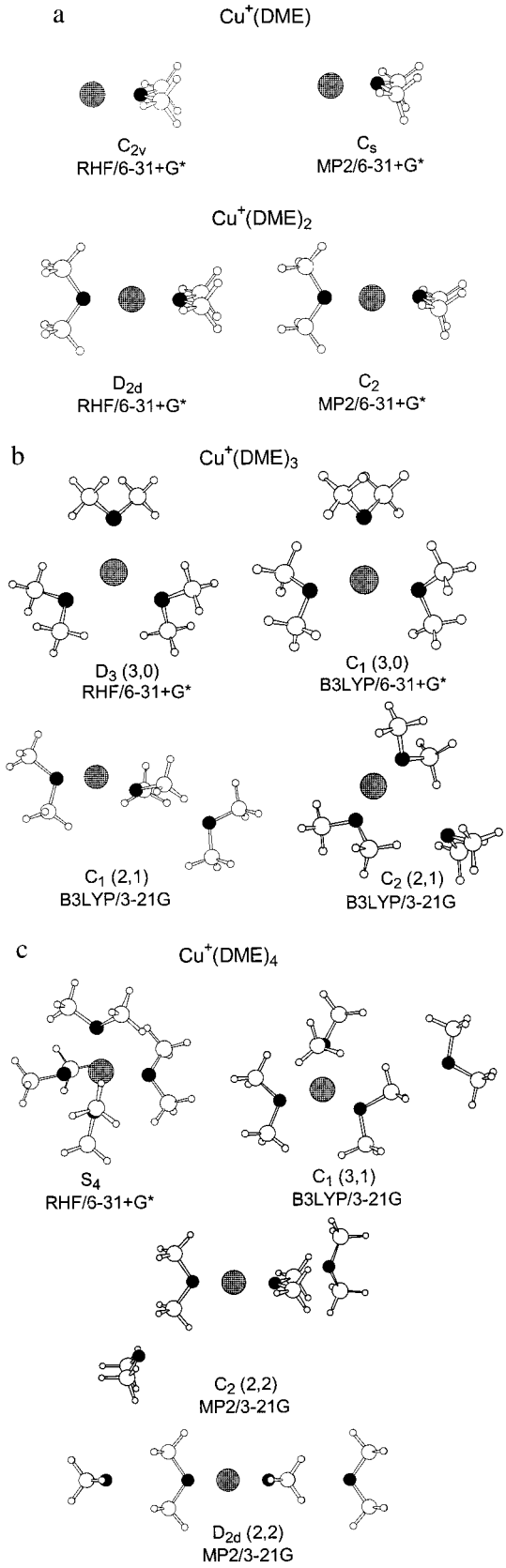

Figure 2. The optimized geometries of $Cu^+(DME)_n$, $n = 1$ and 2 (part a), $n = 3$ (part b), and $n = 4$ (part c) at the indicated level of theory.

For $Cu^+(DME)_2$, the complexes have D_{2d} symmetry at the RHF/6-31+G* level, comparable to the alkali metal DME complexes.[3−7] However, just as Feller and co-workers pointed out for $Cu^+(H_2O)_2$, MP2/3-21G, B3LYP/3-21G, MP2/6-31+G*, and B3LYP/6-31+G* geometry searches find a C_2 geometry complex as the stationary point for $Cu^+(DME)_2$, Figure 2a. In these systems, the Cu^+-O bonds lie out of the C−O−C planes by 22.5° (14.1°) at MP2/6-31+G* (B3LYP/6-31+G*) levels of theory. The MP2 Cu^+-O bond length (Table 3) is 0.043 Å shorter than in the corresponding B3LYP optimized geometry. The magnitude of the displacement vector was large even when the root-mean-squared force was small, indicating that the potential energy surface is flat. The stability gained by relaxing the geometry from D_{2d} to C_2 is only 0.014 (0.0017) eV at the MP2/6-31+G* (B3LYP/6-31+G*) levels of theory. As for the Cu^+(DME) complex, differences in the bond energies for the symmetric D_{2d} and distorted C_2 geometries are small, well within any absolute theoretical uncertainties.

Several conformers for $Cu^+(DME)_3$ are shown in Figure 2b and are denoted as S (J, K) where S stands for the symmetry group (# means a similar symmetry but not exact), J stands for the number of oxygen atoms directly connected to the metal, and K stands for the number of oxygen atoms in a second solvent shell. The first conformer has D_3 (3,0) symmetry and is the ground state conformer at the RHF/3-21G and RHF/6-31+G* levels. Here, the metal ion is aligned with the dipole moments of all three ligands. Four conformers are identified at the B3LYP/3-21G level: C_1 (3,0), D_3 #(3,0), C_2 (2,1), and C_1 (2,1) with relative energies of 0.0, 0.1, 0.5, and 0.6 eV, respectively. The primary distortion in the D_3 #(3,0) complex is that the Cu^+ lies 0.227 Å out of the plane defined by the three oxygen atoms. The relative stability of the conformers in which all DME ligands are in the first solvation shell differ from results for the $Cu^+(H_2O)_3$ complex where a C_1 (2,1) structure is lower in energy than D_3 (3,0) by 0.17 eV at the MP2/aug-cc-pVDZ level.[11] The stability of the C_1 (2,1) structure for water ligands is clearly attributable to effective hydrogen bonding which cannot occur for the DME ligands. Single point MP2/3-21G calculations done on all of the isomers calculated at the B3LYP/3-21G levels indicate that geometries in which a DME ligand is bound in the second valence shell are more than 0.37 eV higher in energy than the C_1 (3,0) ground state conformer. As noted above, the 3-21G basis set may be inadequate to accurately describe the (2,1) conformers, but this energy difference is sufficiently large that the expensive calculations necessary to address this issue using larger basis sets were not pursued. Geometry optimizations of the two lowest energy conformers at the B3LYP/6-31+G* level yield Cu^+-O bond lengths in the C_1 (3,0) geometry of 1.964, 1.965, and 2.249 Å, and in the D_3 (3,0) geometry of 2.045 Å for all three bonds (Table 3). One of the $O-Cu^+-O$ bond angles becomes 159.0° in the C_1 (3,0) geometry, and the Cu^+-O bonds of the two DME ligands with the short Cu^+-O bonds lie out of the C−O−C planes by 26.5°. At the B3LYP/6-31+G*//B3LYP/6-31+G* and MP2/S-hybrid//B3LYP/6-31+G* levels of theory, the energy differences between the ground C_1 (3,0) and excited D_3 (3,0) conformers are 0.05 and 0.11 eV, respectively.

The $Cu^+(DME)_4$ complex also has several stationary points. The highly symmetric S_4 (4,0) structure is a stationary point at the RHF/6-31+G* level of theory, Figure 2c. Feller and co-workers reported C_1 (3,1), C_2 (4,0), and C_2 (2,2) conformers for the $Cu^+(H_2O)_4$ complex at the MP2/aug-cc-pVDZ level of theory.[11] At a B3LYP/3-21G level of theory, we found a stable C_1 (3,1) conformer, Figure 2c. The interactions between a DME ligand in the first solvation shell and one in the second valence shell are expected to be smaller than direct metal−ligand interactions, as found for $n = 3$. The energy of the C_1 (3,1) conformer is 0.17 eV higher than the S_4 (4,0) conformer at a MP2/3-21G//B3LYP/3-21G level of theory. To examine this for

TABLE 4: Theoretical Bond Energies (eV) for $Cu^+(DME)_n$ Complexes[a]

	$n = 1$	$n = 2$	$n = 3$	$n = 4$
B3LYP/6-31+G*//B3LYP/6-31+G*	2.05 (C_{2v})	1.89 (D_{2d})	0.38 (D_3)	0.33 (S_4)
MP2/S-hybrid//B3LYP/6-31+G*	1.88 (C_{2v})	2.00 (D_{2d})	0.40 (D_3)	
MP2/6-31+G*//MP2/6-31+G*	1.88 (C_{2v})	1.89 (D_{2d})		
B3LYP/S-hybrid//B3LYP/S-hybrid[b]	2.05 (C_{2v})	1.91 (D_{2d})	0.45 (D_3)	0.37 (S_4)
B3P86/S-hybrid//B3P86/S-hybrid[b]	2.08 (C_{2v})	1.96 (D_{2d})	0.50 (D_3)	0.40 (S_4)
MP2/S-hybrid//B3LYP/S-hybrid	1.94 (C_{2v})	1.93 (D_{2d})	0.42 (D_3)	0.41 (S_4)
B3LYP/L-hybrid//B3LYP/L-hybrid[b]	2.10 (C_{2v})	1.94 (D_{2d})		
B3P86/L-hybrid//B3P86/L-hybrid[b]	2.10 (C_{2v})	1.98 (D_{2d})		
MP2/L-hybrid//MP2/L-hybrid	1.92 (C_{2v})	1.93 (D_{2d})		
MP4/L-hybrid//MP2/L-hybrid	2.08 (C_{2v})	2.20 (D_{2d})		
B3LYP/6-31+G*//B3LYP/6-31+G*	2.05 (C_s)	1.89 (C_2)	0.43 (C_1)	
MP2/S-hybrid//B3LYP/6-31+G*	1.92 (C_s)	1.92 (C_2)	0.52 (C_1)	
MP2/6-31+G*//MP2/6-31+G*	1.88 (C_s)	1.89 (C_2)		
MP2/S-hybrid//MP2/6-31+G*	1.93 (C_s)	1.94 (C_2)		
Experiment	1.92 ± 0.12	2.00 ± 0.08	0.57 ± 0.04	0.47 ± 0.10

[a] All values corrected for ZPE using frequencies in Table 1. [b] No BSSE corrections.

a C_2 (2,2)-like structure, we attach two DME ligands, optimized at the MP2/3-21G level, onto a $Cu^+(DME)_2$ complex, also optimized at the MP2/3-21G level. Then, we optimize the position of the additional two frozen DME ligands with respect to a frozen $Cu^+(DME)_2$ core, Figure 2c. Compared to Cu^+-$(DME)_4$ complexes having S_4 symmetry, the C_2 (2,2) structure is 1.02 eV higher in energy and the D_{2d} (2,2) is 1.07 eV higher. Therefore, we conclude that all DMEs are likely to be in first solvation shell, but possible distortions from the symmetric S_4 complex at higher levels of correlation with larger basis sets were not investigated because of the computational expense.

All Cu^+−O bond lengths and O−Cu^+−O bond angles optimized by the methods described above are listed in Table 3. The effect of basis set on complex geometry shows several systematic trends. For the $n = 1$ and 2 complexes, B3LYP and RHF methods show an increase in Cu^+−O bond length as the size of the basis set increases, whereas MP2 methods exhibit a decreasing bond length. For $n = 3$ and 4, the same trend is observed for RHF methods, but the B3LYP values show very slight decreases. For $n = 1$ and 2, a larger basis set on C and H (L-hybrid#) did not change the Cu^+−O bond lengths for both the B3LYP and B3P86 results; for that matter, differences in the geometries calculated using the S-hybrid and L-hybrid basis sets are quite small. For all complexes, all correlated methods studied here yield shorter Cu^+−O bond lengths than RHF methods with the same basis set. Geometries optimized at the MP2 level have the shortest Cu^+−O bond lengths for $n = 1$ and 2. Bond lengths and COC bond angles calculated using B3P86 are slightly smaller than those calculated using the B3LYP functional for $n = 1$−4. For RHF/6-31+G* optimized geometries, we find that all Cu^+−O bonds are in the C−O−C plane formed by each DME in order to maximize the dipole interaction between the Cu^+ ion and the DME ligands. In contrast, correlated methods yield optimized geometries in which the Cu^+−O bonds do not lie in the C−O−C plane, Figure 2, as discussed above.

D. Experimental and Theoretical Bond Dissociation Energies. The absolute bond dissociation energies (BDEs) for $Cu^+(DME)_n$ measured experimentally are 1.92 ± 0.12, 2.00 ± 0.08, 0.57 ± 0.04, and 0.47 ± 0.10 eV for n = 1−4, respectively. Strong BDEs are observed for the first and second DMEs with the second BDE somewhat stronger than the first. The third and fourth DME ligands bind much more weakly than the first and second DMEs. These experimental BDEs for $Cu^+(DME)_{n-1}$-DME are listed in Table 4 along with calculated values taken from several levels of theory. All theoretical methods reproduce the strong BDEs for $n = 1$ and 2 and substantially weaker BDEs for $n = 3$ and 4. However, DFT methods show a weaker second than first BDE (by an average of 0.14 ± 0.02 eV), whereas MP2 and MP4 calculations show either equal first and second BDES or an increase that reproduces the experimental trend. Arguably our best calculations are the MP2/S-hybrid//B3LYP/6-31+G* theoretical results (those performed with no symmetry restrictions) which deviate from experiment by an average of 0.04 ± 0.04 eV for $n = 1$−3. Use of MP2/6-31+G* geometries for $n = 1$ and 2, which show shorter Cu^+−O bond lengths, increases the bond energies very slightly. Several of the symmetry-restricted calculations differ from experiment by comparable amounts. The biggest difference in the symmetry-restricted and symmetry unrestricted BDEs is for $n = 3$ where breaking symmetry yields an increase of about 0.10 eV, making the bond energy agree much better with experiment. Overall, the absolute magnitudes of the various bond energies are reproduced at essentially all levels of theory, whereas only MP2 and MP4 theoretical BDEs reproduce the observed trends for $n = 1$ and 2.

The failure of DFT to reproduce the experimental difference in the first and second BDE is mirrored in the geometry changes. Table 3 shows that Cu^+−O bond lengths decrease from $n = 1$ to 2 by only 0.02 Å at the B3LYP/6-31+G* level of theory, whereas MP2/6-31+G* optimized bond lengths decrease by 0.05 Å, presumably resulting in a stronger electrostatic bond. However, even when the B3LYP/6-31+G* geometries are used, MP2 calculations yield similar first and second BDEs, whereas B3LYP calculations invert the strength of these two bond energies. These results may indicate that 4s−3dσ hybridization is not as effectively described in DFT calculations as in MPn theory.

However, as noted above, Cu^+ ion complexes may have a convergence problem with respect to the order of the MPn perturbations. Luna and co-workers find that the MPn series shows strong oscillations for the isolated Cu^+ ion and Cu^+ complexes, with negative corrections for MP2 and MP4, and positive corrections for MP3 and MP5.[28] The MP2 corrections are quite large, while those for MP3−5 are smaller but of comparable magnitude to one another, showing that even at this order the MP series is far from converged. Therefore, they concluded that the MPn BDEs are systematically too small.[28] In the present work, this problem may have been corrected by the inclusion of a single set of copper f functions, which is known to make the BDEs stronger for the analogous $Cu^+(H_2O)_x$ systems.[11] Indeed, the results in Table 4 show that symmetry-restricted MP4/L-hybrid//MP2/L-hybrid values overestimate the BDEs by 0.16 and 0.20 eV for $n = 1$ and 2, respectively.

TABLE 5: Absolute Bond Energies at 0 K and Metal−Oxygen Bond Lengths for Various Metal Ligand Complexes[a]

M^+	Li^+		Na^+		Cu^+	
	BDE (eV)	r(M−O) (Å)	BDE (eV)	r(M−O) (Å)	BDE (eV)	r(M−O) (Å)
M^+(DME)	1.71 (0.11)[b]	1.81	0.95 (0.05)[c]	2.19	1.92 (0.12)	1.89
$M^+(DME)_2$	1.25 (0.06)[b]	1.84	0.85 (0.05)[c]	2.22	2.00 (0.08)	1.89
$M^+(DME)_3$	0.92 (0.08)[b]	1.89	0.72 (0.05)[c]	2.26	0.57 (0.04)	1.96, 2.45
$M^+(DME)_4$	0.70 (0.10)[b]	1.98	0.63 (0.04)[c]	2.30	0.47 (0.10)	2.15
$M^+(H_2O)$	1.40 (0.08)[d]	1.85	0.98 (0.08)[e]	2.21	1.63 (0.08)[f]	1.94
$M^+(H_2O)_2$	1.17 (0.10)[g]	1.87	0.85 (0.06)[e]	2.24	1.76 (0.07)[f]	1.91
$M^+(H_2O)_3$	0.97 (0.04)[g]	1.91	0.73 (0.06)[e]	2.26	0.59 (0.08)[f]	1.83[h]
$M^+(H_2O)_4$	0.73 (0.05)[g]	1.96	0.57 (0.06)[e]	2.29	0.56 (0.04)[f]	1.83[h]

[a] Bond lengths are calculated using B3LYP/6-31+G* with all ligands directly bound to the metal cation, except as noted. [b] Ref 3. [c] Ref 5. [d] Ref 38. [e] Ref 8. [f] Ref 12. [g] Ref 37. [h] These bond lengths are calculated using MP2/6-31+G*/ECP + f, taken from the work of Feller et al., ref 11.

IV. Discussion

A. Effect of d Electrons. The Cu^+ ion has a ^1S ($3d^{10}$) ground-state electronic configuration. It has been shown by Bauschlicher and co-workers that the BDE for $(H_2O)Cu^+$-(H_2O) is larger than the BDE for Cu^+-(H_2O) as a result of 4s−3dσ hybridization.[10] As the first ligand approaches the Cu^+ ion, the occupied 3dσ orbital hybridizes with the empty 4s orbital. The 4s−3dσ hybrid localized along the bonding axis is left empty to act as an acceptor orbital for electron density from the ligand. The pair of electrons originally in the 3dσ orbital occupies the 4s−3dσ orbital localized perpendicular to the bonding axis. Thus, hybridization reduces the charge density of the metal along the bonding axis, thereby reducing metal−ligand repulsion and increasing the effective nuclear charge seen by the ligand. Because of the symmetry of the 4s−3dσ hybrid orbitals, a second ligand, located 180° away from the first, can donate electrons to the same empty 4s−3dσ hybrid orbital. Thus, it also feels less repulsion and a higher nuclear charge, while the energetic cost of hybridization is shared by two ligands, such that the overall BDE can increase slightly. Analogous arguments can be used to describe the BDEs for $Cu^+(DME)_n$, $n = 1$ and 2, complexes. It is interesting to note that all of the calculated $(DME)Cu^+$−(DME) bond lengths are shorter than the Cu^+−(DME) bond lengths. This suggests that the 4s−3dσ hybridization becomes more complete or effective upon addition of the second ligand.

For the C_1 (3,0) conformer of the $n = 3$ complex, 4s−3dσ hybridization leads to two of DMEs binding close to the Cu^+ ion: bond lengths of 1.96 Å, somewhat longer than for the $n = 2$ complex, 1.89 Å. The third ligand has a much longer bond length, 2.25 Å, and thus a much weaker BDE. The presence of the third ligand forces the first two DMEs closer together such that the O−Cu^+−O bond angle is 159°, rather than 180°, Figure 2b. Nevertheless, by retaining some 4s−3dσ hybridization, the complex is more stable by 0.05−0.11 eV compared to the D_3 (3,0) conformer where the O−Cu^+−O bond angles are all 120°. The symmetry of the D_3 (3,0) conformer requires that there is no 4s−3dσ hybridization. Likewise, the symmetry of the S_4 (4,0) ground state conformer of $Cu^+(DME)_4$ can have no residual 4s−3dσ hybridization. Thus, the fourth BDE is again fairly weak.

B. Comparison with Alkali Metal DME Clusters. The influence of 4s−3dσ hybridization on the bonding in the complexes can be further ascertained by comparison to analogous alkali ion DME complexes previously studied by Ray et al.[3,4] and More et al.[5−7] This comparison is particularly relevant when it is realized that the alkali metal ions, like Cu^+, are spherically symmetric with ^1S ground electronic states. The BDEs for these complexes are listed in Table 5 along with metal−oxygen bond lengths calculated at the same level of theory, B3LYP/6-31+G*. For $M^+(DME)_m$ systems where M = any alkali metal, the BDEs decrease almost linearly as m increases, in contrast to the pattern observed for the $Cu^+(DME)_n$ systems, Figure 3. Even though Na^+ and Cu^+ have similar metal ionic radii (0.98 and 0.96 Å, respectively), the first and second DME ligands bind much more strongly to Cu^+ than to Na^+. Compared to sodium ion complexes, much smaller bond lengths are observed in copper ion complexes for $n = 1$ and 2 because of the 4s−3dσ hybridization. Indeed, the first and second DME ligands bind more strongly to Cu^+ than the much smaller Li^+ ion (0.68 Å) despite longer bond lengths because 4s−3dσ hybridization effectively reduces the charge density along the bonding axis and increases the effective charge seen by the ligand. Further, this means that the M−O bond lengths in Cu^+-$(DME)_2$ are similar to those in Cu^+(DME), while in the alkali systems, the M−O bond lengths increase upon addition of a second ligand.

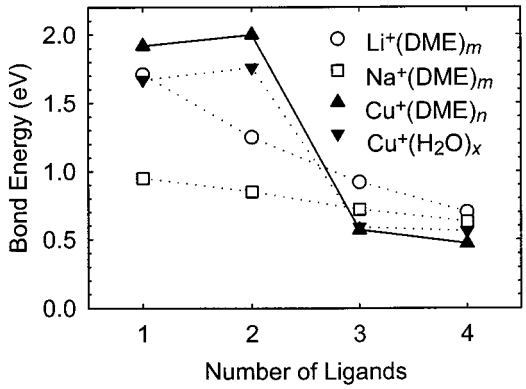

Figure 3. Bond dissociation energies of $Cu^+(DME)_n$ complexes compared to those for $Li^+(DME)_m$, $Na^+(DME)_m$, and $Cu^+(H_2O)_x$ as a function of the number of ligands. Values are taken from Table 5.

In contrast, the third and forth DME bind more weakly to Cu^+ than to Na^+, Figure 3 and Table 5. In $Cu^+(DME)_3$, our calculations indicate one weakly bound ligand located well away from a distorted $Cu^+(DME)_2$ complex. The metal−oxygen bond length for this third ligand (2.45 Å) is considerably longer than those in the symmetric $Na^+(DME)_3$ complex, 2.26 Å; however, the two DME ligands benefiting from 4s−3dσ hybridization still have shorter M−O bond lengths, 1.96 Å. In $Cu^+(DME)_4$, the metal−oxygen bond lengths are shorter than those in the $Na^+(DME)_4$ complex, which has a similar symmetric geometry. This difference appears to conflict with the observation that the $(DME)_3Cu^+$−DME BDE is weaker than the $(DME)_3Na^+$−DME BDE. However, the weak fourth bond in the copper complex is simply a consequence of the strong first and second BDEs, which can be seen by noting that the average BDE for Cu^+-$(DME)_4$ is 1.24 eV, while that for $Na^+(DME)_4$ is 0.79 eV. This trend is consistent with the relative metal−oxygen bond lengths.

C. Comparison with Metal Cation Water Clusters. Previous experimental BDEs[3,5,7,8,12,37,38] for $M^+(DME)_n$ and $M^+(H_2O)_x$ are listed in Table 5 along with theoretical values for the M−O bond lengths, all calculated at the B3LYP/6-31+G* level of theory. The first and second DME ligands are bound to Cu^+ more strongly than analogous water ligands by 0.29 and 0.24 eV, respectively, Figure 3. Further, all of the $M^+(DME)$ and $M^+(DME)_2$ complexes have M−O bond lengths that are shorter than the M−O bond lengths in the analogous water complexes calculated at the same level of theory, Table 5. Previous work[3−7] on analogous alkali metal ion complexes has attributed this to the much larger polarizability of DME (5.24 Å^3)[39,40] than that of H_2O (1.45 Å^3).[41] For Li^+ and Cu^+, which have short M−O bond lengths, these favorable ion induced-dipole interactions (which vary as r^{-4}) overwhelm the contributions from ion−dipole interactions (which vary as r^{-2}) that favor H_2O ($\mu = 1.84$ D)[41] over DME ($\mu = 1.30$ D).[3] Thus, the BDEs of the DME complexes are larger than those of the H_2O complexes, and for the first ligand, the difference is larger for the smaller Li^+ ion. For the second ligand, the difference is much larger for Cu^+, a consequence of the 4s−3dσ hybridization. In contrast, because the M−O bond lengths are longer in the Na^+ complexes, the BDEs of the H_2O complexes are essentially equivalent to those of the DME complexes for both $n = 1$ and 2.

For the third and fourth ligands, the binding nature of the water complexes is completely different from those of the corresponding DME complexes. For water clusters, ground state conformers for $Cu^+(H_2O)_3$ and $Cu^+(H_2O)_4$ are C_1 (2,1) and C_2 (2,2), respectively.[11] Here, the third and fourth ligands form hydrogen bonds with the water ligands in the first solvation shell, which are strongly polarized because of the positive charge on Cu^+ cation. As noted above, DME ligands cannot engage in such strong hydrogen bonding, hence, the third and fourth ligands attach directly to the metal ion. This difference in geometries results in BDEs for the third and fourth water that are slightly larger than those of the corresponding DME ligands.

V. Conclusion

Kinetic energy dependent collision-induced dissociation in a guided ion beam mass spectrometer is used to determine the absolute bond energies of $Cu^+(DME)_n$ for $n = 1-4$. Effects of multiple collisions, internal energies of the complexes, reactant translational distributions, and dissociation lifetimes are all considered in the analysis of the experiments. Our experimental results show strong BDEs for $n = 1$ and 2, increasing slightly for $n = 2$, and much weaker BDEs for $n = 3$ and 4. These trends in the absolute BDEs differ from those for alkali metal cation DME complexes previously studied.[3−7] The trends in the copper complex BDEs and differences from those for the alkali complexes are easily rationalized by 4s−3dσ hybridization. Experimental BDEs for $Cu^+(DME)_n$ complexes are in good agreement with results from MP2 and MP4 calculations, however, B3LYP and B3P86 methods fail to get the right trends in BDEs regardless of the basis set used. The optimized geometry of the $Cu^+(DME)_n$ complexes obtained at the at RHF/6-31+G* level of theory have symmetrically arrayed ligands where the metal ion lies in the plane defined by the C−O−C of the ether ligands. Correlated methods (B3LYP and MP2) find distortions from these symmetric geometries such that the metal no longer lies in the C−O−C plane. Further, we find that the B3LYP/6-31+G* optimized geometry of $Cu^+(DME)_3$ shows residual benefits from 4s−3dσ hybridization, in that two of the DME ligands are close to the metal ion and located 159° from one another, while the third ligand has a much longer Cu−O bond length than the other two. Such higher level calculations were not pursued for the $Cu^+(DME)_4$ complex because of the computational expense.

Acknowledgment. This work is supported by the National Science Foundation, Grant No. CHE-9877162. We thank Prof. Jack Simons, Dr. Alex. Boldyrev, and Dr. Anita Orendt for help running the Gaussian 98 program. H. K. thanks Jay Amicangelo, Rohana Liyanage, Felician Muntean, Chad Rue, and Prof. M. T. Rodgers for their advice throughout these experiments.

References and Notes

(1) Horwitz, E. P.; Dietz, M. L.; Fisher, D. E. *Solvent Extr. Ion Exch.* **1991**, *9*, 1.
(2) Grate, J. W.; Strebin, R.; Janata, J.; Egorov, O.; Ruzicka, J. *J. Anal. Chem.* **1996**, *68*, 333.
(3) Ray, D.; Feller, D.; More, M. B.; Glendening, E. D.; Armentrout, P. B. *J. Phys. Chem.* **1996**, *100*, 1605.
(4) Ray, D.; Feller, D.; More, M. B.; Glendening, E. D.; Armentrout, P. B. *J. Phys. Chem.* **1996**, *100*, 16 116.
(5) More, M. B.; Ray, D.; Armentrout, P. B. *J. Phys. Chem.* **1997**, *101*, 831.
(6) More, M. B.; Ray, D.; Armentrout, P. B. *J. Phys. Chem. A* **1997**, *101*, 4254.
(7) More, M. B.; Ray, D.; Armentrout, P. B. *J. Phys. Chem.* **1997**, *101*, 7007.
(8) Dalleska, N. F.; Tjelta, B. L.; Armentrout, P. B. *J. Phys. Chem.* **1994**, *98*, 4191.
(9) More, M. B.; Ray, D.; Armentrout, P. B. *J. Am. Chem. Soc.* **1999**, *121*, 417.
(10) Bauschlicher, C. W.; Langhoff, S. R.; Partridge, H. *J. Chem. Phys.* **1991**, *94*, 2068.
(11) Feller, D.; Glendening, E. D.; de Jong, W. A. *J. Chem. Phys.* **1999**, *110*, 1475.
(12) Dalleska, N. F.; Honma, K.; Sunderlin, L. S.; Armentrout, P. B. *J. Am. Chem. Soc.* **1994**, *116*, 3519.
(13) Holland, P. M.; Castleman, A. W. *J. Am. Chem. Soc.* **1982**, *76*, 4195
(14) Ervin, K. M.; Armentrout, P. B. *J. Chem. Phys.* **1985**, *83*, 166.
(15) Schultz, R. H.; Armentrout, P. B. *Int. J. Mass Spectrom. Ion Processes* **1991**, *107*, 29.
(16) Schultz, R. H.; Armentrout, P. B. *J. Chem. Phys.* **1992**, *96*, 1046.
(17) Schultz, R. H.; Crellin, K. C.; Armentrout, P. B. *J. Am. Chem. Soc.* **1991**, *113*, 8590.
(18) Khan, F. A.; Clemmer, D. C.; Schultz, R. H.; Armentrout, P. B. *J. Phys. Chem.* **1993**, *97*, 7978.
(19) Mark, S.; Gerlich, D. *J. Chem. Phys.* **1996**, *209*, 235.
(20) Aristov, N.; Armentrout, P. B. *J. Phys. Chem.* **1986**, *90*, 5135.
(21) Gaussian 98, Revision A, Frisch, M. J.; Trucks, G. W.; Schlegel, H. B.; Scuseria, G. E.; Robb, M. A.; Cheeseman, J. R.; Zakrzewski, V. G.; Montgomery, J. A., Jr.; Stratmann, R. E.; Burant, J. C.; Dapprich, S.; Millam, J. M.; Daniels, A. D.; Kudin, K. N.; Strain, M. C.; Farkas, O.; Tomasi, J.; Barone, V.; Cossi, M.; Cammi, R.; Mennucci, B.; Pomelli, C.; Adamo, C.; Clifford, S.; Ochterski, J.; Petersson, G. A.; Ayala, P. Y.; Cui, Q.; Morokuma, K.; Malick, D. K.; Rabuck, A. D.; Raghavachari, K.; Foresman, J. B.; Cioslowski, J.; Ortiz, J. V.; Baboul, A. G.; Stefanov, B. B.; Liu, G.; Liashenko, A.; Piskorz, P.; Komaromi, I.; Gomperts, R.; Martin, R. L ; Fox, D. J.; Keith, T.; Al-Laham, M. A.; Peng, C. Y.; Nanayakkara, A.; Gonzalez, C.; Challacombe, M.; Gill, P. M. W.; Johnson, B.; Chen, W.; Wong, M. W.; Andres, J. L.; Gonzalez, C.; Head-Gordon, M.; Replogle, E. S.; Pople, J. A.; Gaussian, Inc., Pittsburgh, PA, 1998.
(22) Becke, A. D. *J. Chem. Phys.* **1993**, *98*, 5648.
(23) Perdew, J. P. *Phys. Rev.* **1986**, *B 33*, 8822.
(24) Møller, C.; Plesset, M. S. *Physical Review* **1934**, *46*, 618.
(25) *Exploring Chemistry with Electronic Structure Methods*, 2nd ed.; Foresman, J. B.; Frisch, A. E.; Gaussian, Inc.: Pittsburgh, PA, 1996.
(26) Boys, S. F.; Bernardi, F. *Mol. Phys.* **1970**, *19*, 553.
(27) Ghanty, T. K.; Davidson, E. R. *Int. J. Quantum Chemistry* **2000**, *77*, 291.
(28) Luna, A.; Alcami, M.; Mo, O.; Yanez, M. *Chem. Phys. Lett.* **2000**, *320*, 129.
(29) Beyer, T. S.; Swinehart, D. F. *Comm. Assoc. Comput. Machines* **1973**, *16*, 379. Stein, S. E.; Rabinovitch, B. S. *J. Chem. Phys.* **1973**, *58*, 2438. Stein, S. E.; Rabinovitch, B. S. *Chem. Phys. Lett.* **1977**, *49*, 183. Gilbert, R. G.; Smith, S. C. *Theory of Unimolecular and Recombination Reactions*; Blackwell Scientific Publications: Oxford, 1990.
(30) Hales, D. A.; Lian, L.; Armentrout, P. B. *Int. J. Mass Spectrom. Ion Processes* **1990**, *102*, 269.

(31) Marcus, R. A.; Rice, O. K. *J. Phys. Colloid Chem.* **1951**, *55*, 894. Marcus, R. A. *J. Chem. Phys.* **1952**, *20*, 359. Rosenstock, H. M.; Wallenstein, M. B.; Wahrhaftig, A. L.; Eyring, H. *Proc. Natl. Acad. Sci. USA* **1952**, *38*, 667.

(32) Rodgers, M. T.; Ervin, K. M.; Armentrout, P. B. *J. Chem. Phys.* **1997**, *106*, 4499.

(33) Waage, E. V.; Rabinovitch, B. S. *Chem. Rev.* **1970**, *70*, 377.

(34) Boo, B. H.; Armentrout, P. B. *J. Am. Chem. Soc.* **1987**, *109*, 3459. Ervin, K. M.; Armentrout, P. B. *J. Phys. Chem.* **1984**, *88*, 5454. Armentrout, P. B. In *Structure/Reactivity and Thermochemistry of Ions*; Ausloos, P., Lias, S. G. Eds.; Reidel: Dordrecht, 1987; p 97.

(35) Armentrout, P. B.In *Advances in Gas-phase Ion Chemistry*; Adams, N. G., Babcock, L. M., Eds.; JAI: Greenwich, 1992; Vol. 1, p 83.

(36) Armentrout, P. B.; Simons *J. Am. Chem. Soc.* **1992**, *114*, 8627.

(37) Rodgers, M. T.; Armentrout, P. B. *J. Phys. Chem.* **1997**, *101*, 1238.

(38) Rodgers, M. T.; Armentrout, P. B. *J. Chem. Phys.* **1998**, *109*, 1787.

(39) Ramaswarmy, K. L. *Proc. Indian Acad. Sci., Sect. A* **1936**, *4*, 675.

(40) Stuart, H. A. *Die Struktur des Freien Molekuls*; Springer-Verlag: Berlin, 1952; p 441.

(41) Rothe, E. W.; Bernstein, R. B. *J. Chem. Phys.* **1959**, *31*, 1619.